Available online at www.sciencedirect.com
ScienceDirect
Comput. Methods Appl. Mech. Engrg. 307 (2016) 32–43
Computer methods in applied mechanics and engineering
www.elsevier.com/locate/cma

A simple and efficient finite difference method for the phase-field crystal equation on curved surfaces

Hyun Geun Lee[a], Junseok Kim[b,*]

[a] *Institute of Mathematical Sciences, Ewha Womans University, Seoul 120-750, Republic of Korea*
[b] *Department of Mathematics, Korea University, Seoul 136-713, Republic of Korea*

Received 19 February 2016; received in revised form 11 April 2016; accepted 18 April 2016
Available online 26 April 2016

Highlights

- A simple and efficient finite difference method for the phase-field crystal equation on curved surfaces is presented.
- The proposed method can be combined with any time discretization.
- The proposed method gives stable solutions even on the surface having sharp curvatures without difficulties.

Abstract

We present a simple and efficient finite difference method for the phase-field crystal (PFC) equation on curved surfaces embedded in $\mathbb{R}^3$. We employ a narrow band neighborhood of a curved surface that is defined as a zero level set of a signed distance function. The PFC equation on the surface is extended to the three-dimensional narrow band domain. By using the closest point method and applying a pseudo-Neumann boundary condition, we can use the standard seven-point discrete Laplacian operator instead of the discrete Laplace–Beltrami operator on the surface. The PFC equation on the narrow band domain is discretized using an unconditionally stable scheme and the resulting implicit discrete system of equations is solved by using the Jacobi iterative method. Computational results are presented to demonstrate the efficiency and usefulness of the proposed method.

Keywords: Phase-field crystal equation; Curved surface; Finite difference method; Narrow band domain; Closest point method

1. Introduction

Material properties are controlled by complex microstructures exhibiting topological defects, such as vacancies, grain boundaries, and dislocations. One model for simulating these defects is the phase-field crystal (PFC) equation proposed by Elder et al. [1,2]. This model describes the microstructure of two-phase systems on atomic length scales but on diffusive time scales, leading to significant computational savings compared to molecular dynamics simulations

* Corresponding author. Tel.: +82 2 3290 3077; fax: +82 2 929 8562.
E-mail address: cfdkim@korea.ac.kr (J. Kim).
URL: http://math.korea.ac.kr/~cfdkim (J. Kim).

http://dx.doi.org/10.1016/j.cma.2016.04.022

which are limited by atomic length scales and femtosecond time scales. The PFC equation has been used to study various phenomena, including grain growth, dendritic and eutectic solidification, and epitaxial growth [1,3].

The PFC equation is derived from a free energy functional of Swift–Hohenberg type [4]

$$\mathcal{E}(\phi) := \int_{\Omega} \left(\frac{1}{4}\phi^4 + \frac{1-\epsilon}{2}\phi^2 - |\nabla\phi|^2 + \frac{1}{2}(\Delta\phi)^2 \right) d\mathbf{x}, \tag{1}$$

where $\phi : \Omega \subset \mathbb{R}^d \to \mathbb{R}$ $(d = 1, 2, 3)$ is the density field and ϵ is a positive constant with physical significance. Under the constraint of mass conservation, the PFC equation is given by

$$\frac{\partial\phi}{\partial t} = \Delta\mu, \tag{2}$$

where μ is the chemical potential defined as $\mu := \delta\mathcal{E}/\delta\phi = \phi^3 + (1-\epsilon)\phi + 2\Delta\phi + \Delta^2\phi$ and $\delta\mathcal{E}/\delta\phi$ denotes the variational derivative of $\mathcal{E}$ with respect to ϕ. Because (2) is of gradient type, it is easy to see that the energy functional (1) is non-increasing in time. The PFC equation is a sixth-order nonlinear partial differential equation and cannot generally be solved analytically. Therefore, computer simulations play an essential role in understanding of nonequilibrium processing. Various computational algorithms [1,2,5–13] have been developed to solve the PFC equation numerically. There are a few related works that try to solve the PFC equation on curved surfaces [14–16].

The aim of this paper is to present a simple and efficient finite difference method for the PFC equation on curved surfaces in three-dimensional space. The key element in solving the PFC equation on a curved surface is calculating the Laplace–Beltrami operator for describing the Laplacian on the curved surface [17]. Our method is based on the closest point method [18–20]: we define a narrow band domain of the surface that is represented as a zero level set of a signed distance function. Then, on the boundary of the narrow band domain, we apply a pseudo-Neumann boundary condition via the closest point. This boundary treatment results that the density field ϕ is constant in the direction normal to the surface. Thus, we can use the standard Laplacian operator instead of the Laplace–Beltrami operator. Furthermore, we take the minimum number of grid points for the discrete narrow band domain and solve the PFC equation only on the discrete narrow band domain. Therefore, the algorithm is simple and efficient. Note that our method can be combined with any time discretization, but the Jacobi iterative method is used to solve the resulting implicit discrete system of equations efficiently.

The outline of the paper is as follows. In Section 2, we describe the PFC equation on a narrow band domain. In Section 3, we provide the numerical solution algorithm. Numerical experiments on various curved surfaces are presented in Section 4. Finally, conclusions are drawn in Section 5.

2. Phase-field crystal equation on a narrow band domain

The PFC equation on the surface S in $\mathbb{R}^3$ is given by

$$\frac{\partial\phi(\mathbf{x},t)}{\partial t} = \Delta_S\mu(\mathbf{x},t), \quad \mathbf{x} \in S,\ 0 < t \le T, \tag{3}$$

$$\mu(\mathbf{x},t) = \phi^3(\mathbf{x},t) + (1-\epsilon)\phi(\mathbf{x},t) + 2\Delta_S\phi(\mathbf{x},t) + \Delta_S\nu(\mathbf{x},t), \tag{4}$$

$$\nu(\mathbf{x},t) = \Delta_S\phi(\mathbf{x},t), \tag{5}$$

where Δ_S is the Laplace–Beltrami operator and is defined as $\Delta_S\phi = \nabla\cdot(\mathbf{P}\nabla\phi)$. Here, $\mathbf{P} = \mathbf{I} - (\nabla\psi)^T\nabla\psi$ is a projection operator onto the tangent plane [21,22], where $\mathbf{I}$ is the 3×3 identity matrix and $\psi : \mathbb{R}^3 \to \mathbb{R}$ is a signed distance function such that $S = \{\mathbf{x} \in \mathbb{R}^3 | \psi(\mathbf{x}) = 0\}$ with $\psi < 0$ inside of S and $\psi > 0$ outside of S. Next, let $\Omega_\delta = \{\mathbf{y} | \mathbf{x} \in S, \mathbf{y} = \mathbf{x} + \theta\mathbf{n}(\mathbf{x}) \text{ for } |\theta| < \delta\}$ be a δ-neighborhood band of S, where $\mathbf{n}(\mathbf{x})$ is a unit normal vector at $\mathbf{x}$. Then, we extend the PFC equations (3)–(5) to the narrow band domain Ω_δ:

$$\frac{\partial\phi(\mathbf{x},t)}{\partial t} = \Delta_S\mu(\mathbf{x},t), \quad \mathbf{x} \in \Omega_\delta,\ 0 < t \le T, \tag{6}$$

$$\mu(\mathbf{x},t) = \phi^3(\mathbf{x},t) + (1-\epsilon)\phi(\mathbf{x},t) + 2\Delta_S\phi(\mathbf{x},t) + \Delta_S\nu(\mathbf{x},t), \tag{7}$$

$$\nu(\mathbf{x},t) = \Delta_S\phi(\mathbf{x},t) \tag{8}$$

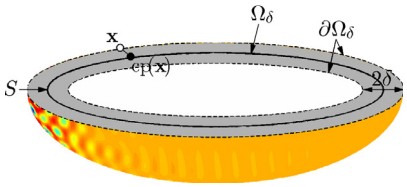

Fig. 1. Schematic illustration of a surface S, a narrow band domain Ω_δ with a thickness of 2δ, its boundary $\partial\Omega_\delta$, and the closest point $\mathrm{cp}(\mathbf{x})$ for a point $\mathbf{x} \in \partial\Omega_\delta$.

with the following pseudo-Neumann boundary condition on $\partial\Omega_\delta$:

$$\phi(\mathbf{x},t) = \phi(\mathrm{cp}(\mathbf{x}),t), \qquad \mu(\mathbf{x},t) = \mu(\mathrm{cp}(\mathbf{x}),t), \quad \text{and} \quad \nu(\mathbf{x},t) = \nu(\mathrm{cp}(\mathbf{x}),t), \tag{9}$$

where $\mathrm{cp}(\mathbf{x})$ is a point on S, which is closest to $\mathbf{x} \in \partial\Omega_\delta$ [20]. Fig. 1 shows a schematic illustration of a surface S, a narrow band domain Ω_δ with a thickness of 2δ, its boundary $\partial\Omega_\delta$, and the closest point $\mathrm{cp}(\mathbf{x})$ for a point $\mathbf{x} \in \partial\Omega_\delta$.

If we take a sufficiently small δ, then we have a constant value of ϕ in the direction normal to the surface. Thus, we can use the standard Laplacian operator instead of the Laplace–Beltrami operator in the narrow band domain Ω_δ [20], i.e., we have

$$\frac{\partial\phi(\mathbf{x},t)}{\partial t} = \Delta\mu(\mathbf{x},t), \quad \mathbf{x} \in \Omega_\delta,\ 0 < t \le T, \tag{10}$$

$$\mu(\mathbf{x},t) = \phi^3(\mathbf{x},t) + (1-\epsilon)\phi(\mathbf{x},t) + 2\Delta\phi(\mathbf{x},t) + \Delta\nu(\mathbf{x},t), \tag{11}$$

$$\nu(\mathbf{x},t) = \Delta\phi(\mathbf{x},t). \tag{12}$$

3. Numerical solution algorithm

In this section, we describe our algorithm for solving Eqs. (10)–(12) with the boundary condition (9). Using ideas presented in [18,19] for the Allen–Cahn equation and the nonlocal Cahn–Hilliard equation, we discretize Eqs. (10)–(12) in the three-dimensional domain $\Omega = [a,b] \times [c,d] \times [e,f]$ that includes Ω_δ. Let $h = (b-a)/N_x = (d-c)/N_y = (f-e)/N_z$ be the uniform grid size, where N_x, N_y, and N_z are positive integers. Let $\Omega^h = \{\mathbf{x}_{ijk} = (x_i, y_j, z_k) | x_i = a + hi, y_j = c + hj, z_k = e + hk \text{ for } 0 \le i \le N_x, 0 \le j \le N_y, 0 \le k \le N_z\}$ be a discrete domain. Let ϕ^n_{ijk} be an approximation of $\phi(\mathbf{x}_{ijk}, n\Delta t)$, where Δt is the time step. Let $\Omega^h_\delta = \{\mathbf{x}_{ijk} | |\psi_{ijk}| < \delta\}$ be a discrete narrow band domain and $\partial\Omega^h_\delta = \{\mathbf{x}_{ijk} | I_{ijk} | \nabla_h I_{ijk}| \neq 0\}$ be discrete domain boundary points, where $\nabla_h I_{ijk} = (I_{i+1,j,k} - I_{i-1,j,k}, I_{i,j+1,k} - I_{i,j-1,k}, I_{i,j,k+1} - I_{i,j,k-1})/(2h)$. Here, $I_{ijk} = 0$ if $\mathbf{x}_{ijk} \in \Omega^h_\delta$, and $I_{ijk} = 1$ otherwise. We discretize Eqs. (10)–(12) by applying an unconditionally stable scheme [12]:

$$\frac{\phi^{n+1}_{ijk} - \phi^n_{ijk}}{\Delta t} = \Delta_h \mu^{n+1}_{ijk}, \tag{13}$$

$$\mu^{n+1}_{ijk} = (\phi^{n+1}_{ijk})^3 + (1-\epsilon)\phi^{n+1}_{ijk} + 2\Delta_h\phi^n_{ijk} + \Delta_h\nu^{n+1}_{ijk}, \tag{14}$$

$$\nu^{n+1}_{ijk} = \Delta_h\phi^{n+1}_{ijk} \tag{15}$$

with the following boundary condition on $\partial\Omega^h_\delta$:

$$\phi^{n+1}_{ijk} = \phi^{n+1}(\mathrm{cp}(\mathbf{x}_{ijk})), \qquad \mu^{n+1}_{ijk} = \mu^{n+1}(\mathrm{cp}(\mathbf{x}_{ijk})), \quad \text{and} \quad \nu^{n+1}_{ijk} = \nu^{n+1}(\mathrm{cp}(\mathbf{x}_{ijk})).$$

Here, $\Delta_h\phi_{ijk} = (\phi_{i+1,j,k} + \phi_{i-1,j,k} + \phi_{i,j+1,k} + \phi_{i,j-1,k} + \phi_{i,j,k+1} + \phi_{i,j,k-1} - 6\phi_{ijk})/h^2$. The numerical closest point $\mathrm{cp}(\mathbf{x}_{ijk})$ for a point $\mathbf{x}_{ijk} \in \partial\Omega^h_\delta$ is defined as

$$\mathrm{cp}(\mathbf{x}_{ijk}) = \mathbf{x}_{ijk} - |\psi_{ijk}| \frac{\nabla_h|\psi_{ijk}|}{|\nabla_h|\psi_{ijk}||}.$$

In general, $\mathrm{cp}(\mathbf{x}_{ijk})$ is not a grid point in Ω^h_δ, i.e., $\mathrm{cp}(\mathbf{x}_{ijk}) \notin \Omega^h_\delta$, and thus we calculate $\phi(\mathrm{cp}(\mathbf{x}_{ijk}))$ by using trilinear interpolation. Therefore, we need to take $\delta > \sqrt{3}h$. In order to solve the implicit discrete equations (13)–(15)

efficiently, we use the Jacobi iterative method: we set an initial guess $\{\phi_{ijk}^{n+1,0}, \mu_{ijk}^{n+1,0}, \nu_{ijk}^{n+1,0}\} = \{\phi_{ijk}^{n}, \mu_{ijk}^{n}, \nu_{ijk}^{n}\}$ and calculate $\{\phi_{ijk}^{n+1,m+1}, \mu_{ijk}^{n+1,m+1}, \nu_{ijk}^{n+1,m+1}\}$ from the given $\{\phi_{ijk}^{n+1,m}, \mu_{ijk}^{n+1,m}, \nu_{ijk}^{n+1,m}\}$ for $m = 0, 1, \ldots$, by solving the following equations: for all $\mathbf{x}_{ijk} \in \Omega_\delta^h$,

$$\frac{\phi_{ijk}^{n+1,m+1}}{\Delta t} + \frac{6\mu_{ijk}^{n+1,m+1}}{h^2} = \frac{\phi_{ijk}^{n}}{\Delta t} + \frac{\mu_{i+1,j,k}^{n+1,m} + \mu_{i-1,j,k}^{n+1,m} + \mu_{i,j+1,k}^{n+1,m} + \mu_{i,j-1,k}^{n+1,m} + \mu_{i,j,k+1}^{n+1,m} + \mu_{i,j,k-1}^{n+1,m}}{h^2}, \tag{16}$$

$$\begin{aligned} &\times \left[-3(\phi_{ijk}^{n+1,m})^2 - 1 + \epsilon\right]\phi_{ijk}^{n+1,m+1} + \mu_{ijk}^{n+1,m+1} + \frac{6\nu_{ijk}^{n+1,m+1}}{h^2} \\ &= \frac{2(\phi_{i+1,j,k}^{n} + \phi_{i-1,j,k}^{n} + \phi_{i,j+1,k}^{n} + \phi_{i,j-1,k}^{n} + \phi_{i,j,k+1}^{n} + \phi_{i,j,k-1}^{n} - 6\phi_{ijk}^{n})}{h^2} \\ &\quad - 2(\phi_{ijk}^{n+1,m})^3 + \frac{\nu_{i+1,j,k}^{n+1,m} + \nu_{i-1,j,k}^{n+1,m} + \nu_{i,j+1,k}^{n+1,m} + \nu_{i,j-1,k}^{n+1,m} + \nu_{i,j,k+1}^{n+1,m} + \nu_{i,j,k-1}^{n+1,m}}{h^2}, \end{aligned} \tag{17}$$

$$\frac{6\phi_{ijk}^{n+1,m+1}}{h^2} + \nu_{ijk}^{n+1,m+1} = \frac{\phi_{i+1,j,k}^{n+1,m} + \phi_{i-1,j,k}^{n+1,m} + \phi_{i,j+1,k}^{n+1,m} + \phi_{i,j-1,k}^{n+1,m} + \phi_{i,j,k+1}^{n+1,m} + \phi_{i,j,k-1}^{n+1,m}}{h^2}. \tag{18}$$

We iterate the Jacobi iteration (16)–(18) until $\|\phi^{n+1,m+1} - \phi^{n+1,m}\|_{L^2(\Omega_\delta^h)}$ is less than a tolerance tol. Here, a discrete L^2-norm on Ω_δ^h is defined as $\|\phi\|_{L^2(\Omega_\delta^h)} = \sqrt{\sum_{\mathbf{x}_{ijk}\in\Omega_\delta^h} \phi_{ijk}^2 / \#\Omega_\delta^h}$, where $\#\Omega_\delta^h$ is the number of elements in the set Ω_δ^h. Then, we set $\{\phi_{ijk}^{n+1,*}, \mu_{ijk}^{n+1,*}, \nu_{ijk}^{n+1,*}\} = \{\phi_{ijk}^{n+1,m+1}, \mu_{ijk}^{n+1,m+1}, \nu_{ijk}^{n+1,m+1}\}$. Finally, $\sum_{\mathbf{x}_{ijk}\in\Omega_\delta^h} \phi_{ijk}^{n} / \#\Omega_\delta^h$ is generally not constant with respect to n since the boundary condition (9) is not conservative. In order to make the method conservative, the following correction procedure is used:

$$\phi_{ijk}^{n+1} = \phi_{ijk}^{n+1,*} + \frac{1}{\#\Omega_\delta^h} \sum_{\mathbf{x}_{pqr}\in\Omega_\delta^h} (\phi_{pqr}^{0} - \phi_{pqr}^{n+1,*}) \quad \text{for all } \mathbf{x}_{ijk} \in \Omega_\delta^h.$$

4. Numerical experiments

We perform several numerical experiments on various curved surfaces. Unless otherwise stated, we take an initial condition as

$$\phi(x, y, z, 0) = \bar{\phi} + \text{rand}(x, y, z),$$

where $\text{rand}(x, y, z)$ is a random number between -0.1 and 0.1. The parameters $h = \Delta t = 1$, $\epsilon = 0.25$, $\delta = 1.1\sqrt{3}h$, and $tol = 0.1$ are used.

4.1. Convergence test

In order to estimate the convergence rate with respect to h, we consider the evolution of ϕ on a unit sphere. An initial condition is

$$\phi(x, y, z, 0) = 0.5 \sin(2\pi x) \sin(2\pi y) \sin(2\pi z)$$

and the unit sphere is represented as a zero level set of the following signed distance function:

$$\psi(x, y, z) = \sqrt{x^2 + y^2 + z^2} - 1$$

on a domain $\Omega = [-1.5, 1.5]^3$. Simulations are performed by varying $h = 0.2, 0.1, 0.05, 0.025, 0.0125$. The time steps are $\Delta t = 0.1h^2$. We define the L^2- and L^∞-errors between two different grid sizes h and $h/2$ to be

$$\|\phi^{h,\Delta t} - \phi^{h/2,\Delta t/4}\|_{L^2(\Omega_\delta^{h/2})} = \sqrt{\sum_{\mathbf{x}_{ijk}\in\Omega_\delta^{h/2}} \left(\phi_{ijk}^{h,\Delta t} - \phi_{2i-1,2j-1,2k-1}^{h/2,\Delta t/4}\right)^2 / \#\Omega_\delta^{h/2}}$$

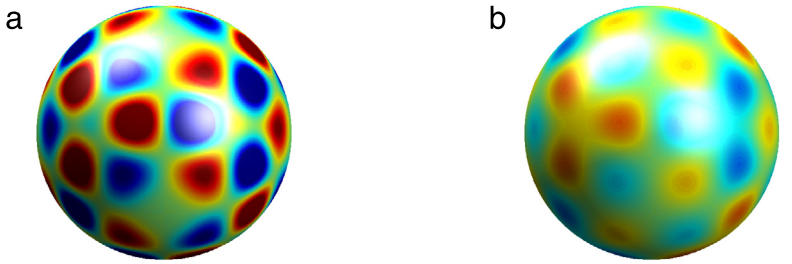

Fig. 2. (a) $\phi(x, y, z, 0)$ and (b) $\phi(x, y, z, 0.008)$ with $h = 0.0125$. The red, green, and blue regions indicate $\phi = 0.25$, 0, and -0.25, respectively. (For interpretation of the references to color in this figure legend, the reader is referred to the web version of this article.)

Table 1
L^2- and L^∞-errors and convergence rates at $t = 0.008$.

h	0.2–0.1		0.1–0.05		0.05–0.025		0.025–0.0125
L^2-error	3.849×10^{-2}		1.150×10^{-2}		3.132×10^{-3}		7.105×10^{-4}
Rate		1.74		1.88		2.14	
L^∞-error	8.304×10^{-2}		2.709×10^{-2}		6.897×10^{-3}		1.461×10^{-3}
Rate		1.62		1.97		2.24	

and

$$\|\phi^{h,\Delta t} - \phi^{h/2,\Delta t/4}\|_{L^\infty(\Omega_\delta^{h/2})} = \max_{\mathbf{x}_{ijk} \in \Omega_\delta^{h/2}} \left| \phi_{ijk}^{h,\Delta t} - \phi_{2i-1,2j-1,2k-1}^{h/2,\Delta t/4} \right|,$$

respectively. Here, $\phi^{h,\Delta t}$ is a numerical solution obtained with a grid size h and a time step Δt. The convergence rate is defined as

$$\log_2 \left(\frac{\|\phi^{h,\Delta t} - \phi^{h/2,\Delta t/4}\|}{\|\phi^{h/2,\Delta t/4} - \phi^{h/4,\Delta t/16}\|} \right).$$

Fig. 2(a) and (b) show $\phi(x, y, z, 0)$ and $\phi(x, y, z, 0.008)$ with $h = 0.0125$, respectively. The errors and convergence rates at $t = 0.008$ are shown in Table 1. The results suggest that the numerical scheme is approximately second-order accurate in space and first-order accurate in time. Note that we applied the pseudo-Neumann boundary condition $\phi_{ijk} = \phi(\text{cp}(\mathbf{x}_{ijk}))$ on $\partial\Omega_\delta^h$ and calculated $\phi(\text{cp}(\mathbf{x}_{ijk}))$ by an interpolation since $\text{cp}(\mathbf{x}_{ijk}) \notin \Omega_\delta^h$. Thus, the order of the numerical scheme can be affected by this implementation. In order to obtain more accurate results, one can try the method suggested in [20]. Fig. 3 shows the evolution of the energy for various grid sizes. We observe that the energy is non-increasing.

4.2. Temporal evolution on a sphere

Next, we consider the evolution of ϕ on a sphere. The sphere is represented as a zero level set of the following signed distance function:

$$\psi(x, y, z) = \sqrt{x^2 + y^2 + z^2} - 64$$

on a domain $\Omega = [-68, 68]^3$. Figs. 4 and 5 show the evolution of $\phi(x, y, z, t)$ with $\bar{\phi} = 0.05$ and 0.15, respectively. Depending on the value of $\bar{\phi}$, we have different patterns, such as striped (Fig. 4) and hexagonal (Fig. 5). Fig. 6 shows the evolution of the energy with $\bar{\phi} = 0.05$ and 0.15. We observe that the energy is non-increasing.

4.3. Temporal evolution on a sphere perturbed by a spherical harmonic

In this section, we validate that the proposed method can handle complex surfaces by simulating the evolution of ϕ on a sphere of center $(0, 0, 0)$ and radius 32 perturbed by a spherical harmonic $10Y_{10}^7(\theta, \varphi)$. Here, θ and φ are the

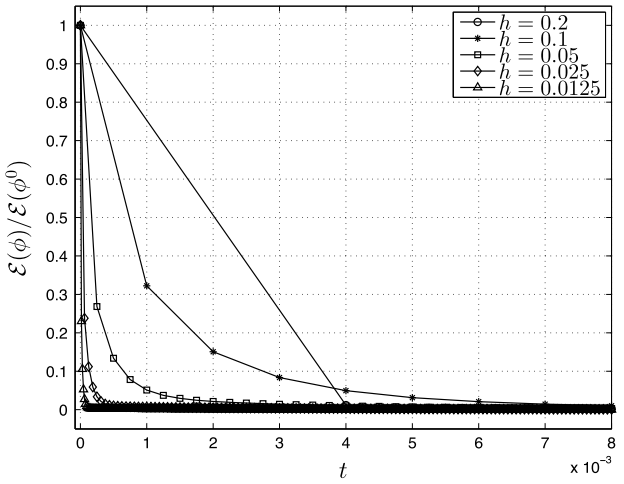

Fig. 3. Evolution of $\mathcal{E}(\phi)/\mathcal{E}(\phi^0)$ for various grid sizes.

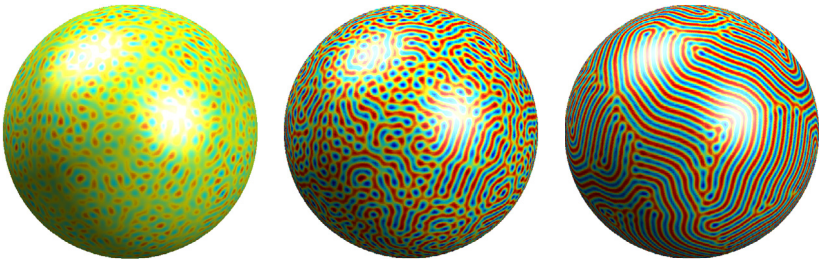

(a) $t = 200$. (b) $t = 500$. (c) $t = 10{,}000$.

Fig. 4. Evolution of $\phi(x, y, z, t)$ with $\bar{\phi} = 0.05$.

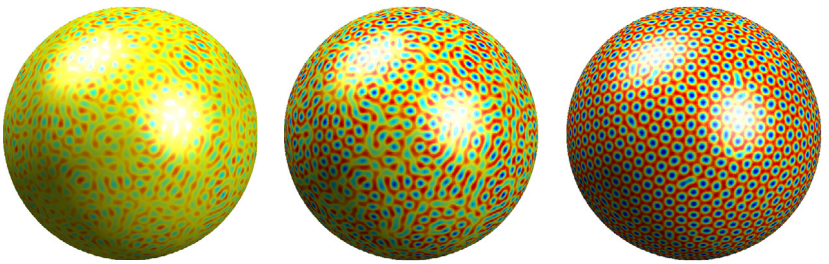

(a) $t = 250$. (b) $t = 350$. (c) $t = 5000$.

Fig. 5. Evolution of $\phi(x, y, z, t)$ with $\bar{\phi} = 0.15$.

polar and azimuthal angles, respectively, and the computational domain is $\Omega = [-40, 40]^3$. Figs. 7 and 8 show the evolution of $\phi(x, y, z, t)$ with $\bar{\phi} = 0.05$ and 0.15, respectively. From the results in Figs. 7 and 8, we can see that our method can solve the PFC equation on not only simple but also complex surfaces. Fig. 9 shows the evolution of the energy with $\bar{\phi} = 0.05$ and 0.15. We observe that the energy is non-increasing.

4.4. Temporal evolution on a cube

In order to demonstrate the robustness of the proposed method, we consider the evolution of ϕ on a cube that has sharp curvatures. The cube is represented as a zero level set of the following signed distance function:

$$\psi(x, y, z) = \min(\max(\bar{x}, \max(\bar{y}, \bar{z})), 0) + \sqrt{\max(\bar{x}, 0)^2 + \max(\bar{y}, 0)^2 + \max(\bar{z}, 0)^2}$$

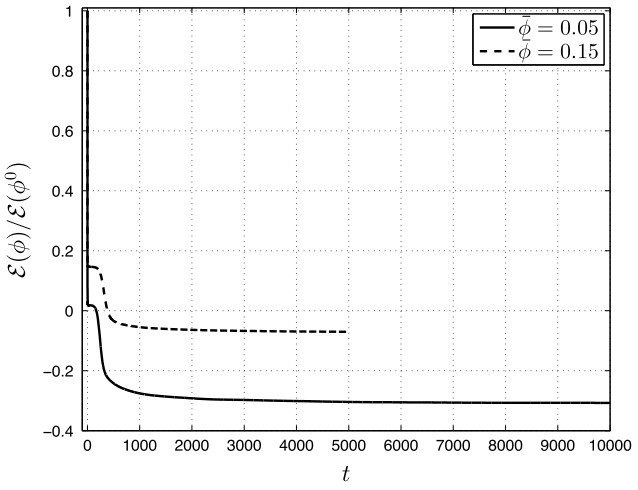

Fig. 6. Evolution of $\mathcal{E}(\phi)/\mathcal{E}(\phi^0)$ with $\bar{\phi} = 0.05$ and 0.15.

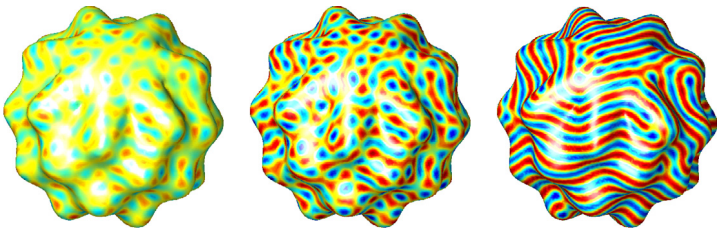

(a) $t = 200$. (b) $t = 300$. (c) $t = 10{,}000$.

Fig. 7. Evolution of $\phi(x, y, z, t)$ with $\bar{\phi} = 0.05$.

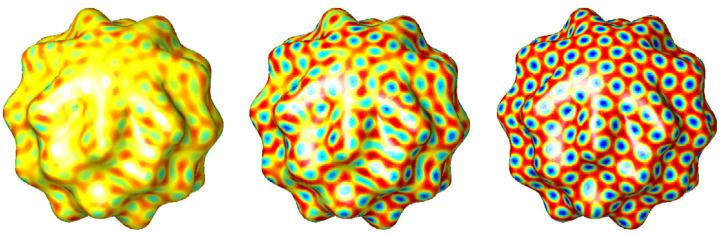

(a) $t = 250$. (b) $t = 350$. (c) $t = 5000$.

Fig. 8. Evolution of $\phi(x, y, z, t)$ with $\bar{\phi} = 0.15$.

on a domain $\Omega = [-36, 36]^3$, where $\bar{x} = |x| - 32$, $\bar{y} = |y| - 32$, and $\bar{z} = |z| - 32$. Figs. 10 and 11 show the evolution of $\phi(x, y, z, t)$ with $\bar{\phi} = 0.05$ and 0.15, respectively. As we can see in Figs. 10 and 11, our method gives stable solutions without difficulties, even on a surface having sharp curvatures. Fig. 12 shows the evolution of the energy with $\bar{\phi} = 0.05$ and 0.15. We observe that the energy is non-increasing.

4.5. Crystal growth in a supercooled liquid on an ellipsoid

Droplets of supercooled water often exist in stratiform and cumulus clouds. Abrupt crystallization of these droplets can occur when aircraft fly through these clouds, which can result in the formation of ice on the aircraft's wings or blockage of its instruments and probes. In order to simulate aircraft icing, we consider crystal growth in a supercooled liquid on an ellipsoid. We take an initial condition

$$\phi(x, y, z, 0) = \begin{cases} 0.285 + \text{rand}(x, y, z) & \text{if } x < -60 \\ 0.285 & \text{otherwise} \end{cases}$$

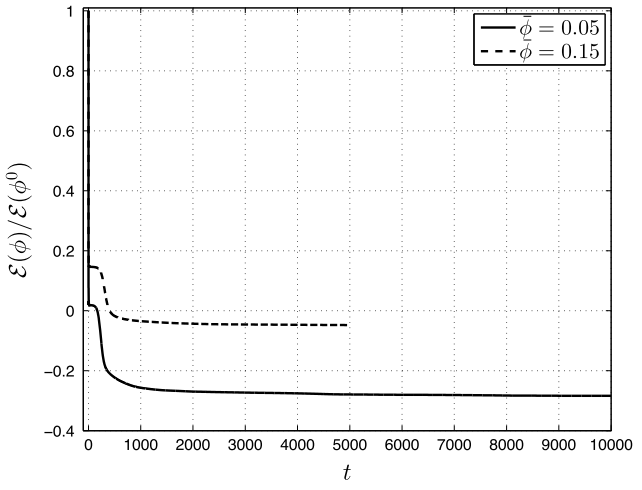

Fig. 9. Evolution of $\mathcal{E}(\phi)/\mathcal{E}(\phi^0)$ with $\bar{\phi} = 0.05$ and 0.15.

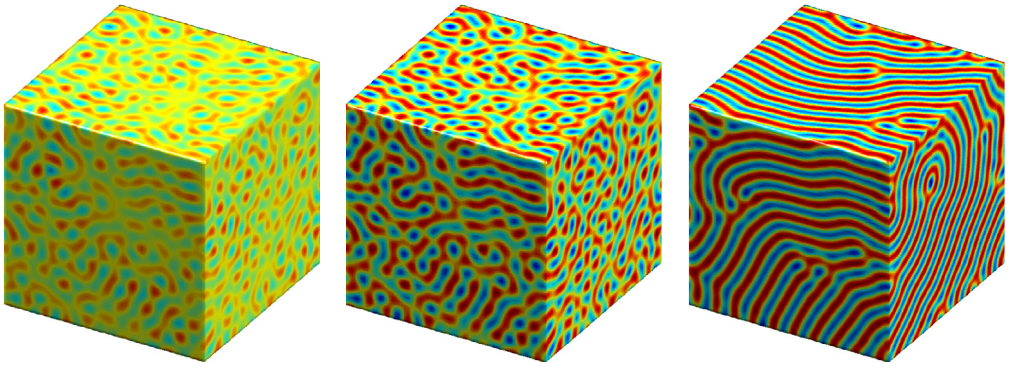

(a) $t = 200$. (b) $t = 300$. (c) $t = 10{,}000$.

Fig. 10. Evolution of $\phi(x, y, z, t)$ with $\bar{\phi} = 0.05$.

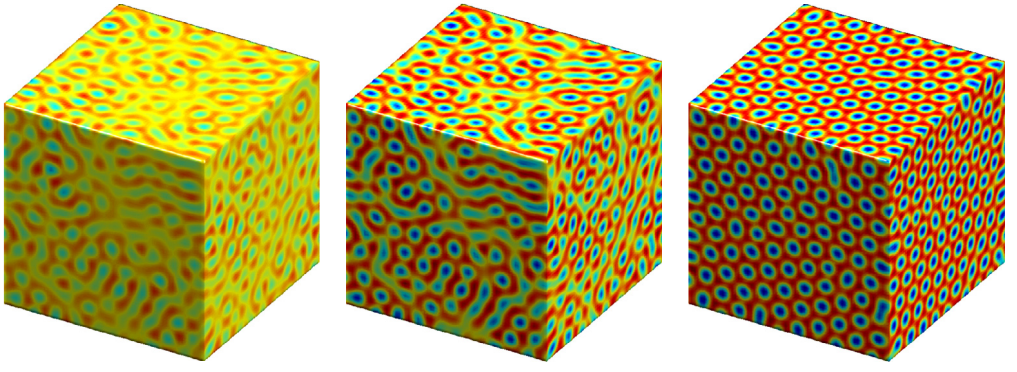

(a) $t = 250$. (b) $t = 350$. (c) $t = 5000$.

Fig. 11. Evolution of $\phi(x, y, z, t)$ with $\bar{\phi} = 0.15$.

on a domain $\Omega = [-68, 68] \times [-36, 36] \times [-36, 36]$. Fig. 13 shows the evolution of $\phi(x, y, z, t)$ on an ellipsoid of center $(0, 0, 0)$ and radius $(64, 32, 32)$. We observe the growth of a crystalline phase and the motion of a well-defined crystal–liquid interface. Fig. 14 shows the evolution of the energy. We observe that the energy is non-increasing.

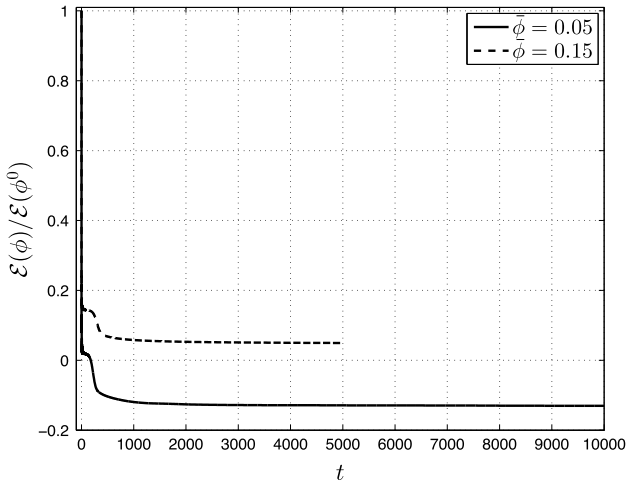

Fig. 12. Evolution of $\mathcal{E}(\phi)/\mathcal{E}(\phi^0)$ with $\bar{\phi} = 0.05$ and 0.15.

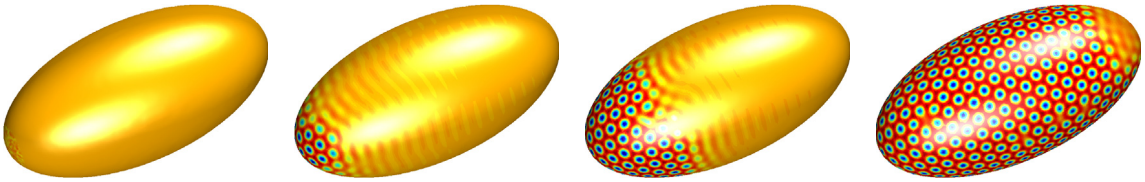

(a) $t = 0$. (b) $t = 8000$. (c) $t = 9000$. (d) $t = 16{,}000$.

Fig. 13. Crystal growth in a supercooled liquid on an ellipsoid.

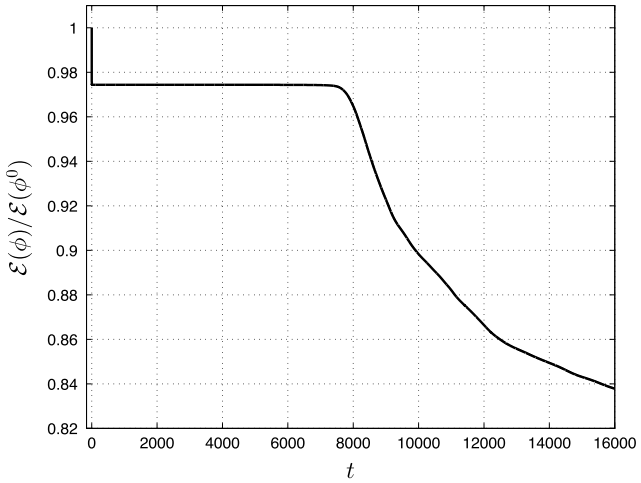

Fig. 14. Evolution of $\mathcal{E}(\phi)/\mathcal{E}(\phi^0)$.

4.6. Mixed pattern on an ellipsoid

In this section, we solve the PFC equation on an ellipsoid of center $(0, 0, 0)$ and radius $(96, 16, 16)$ with the following initial condition:

$$\phi(x, y, z, 0) = 0.05 + (0.285 - 0.05)\left(\frac{x + 100}{200}\right)^3 + \text{rand}(x, y, z).$$

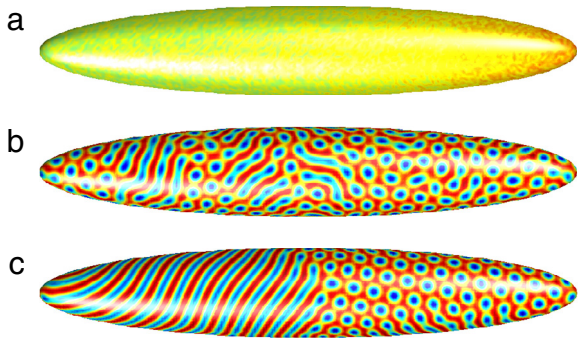

Fig. 15. Evolution of $\phi(x, y, z, t)$ at (a) $t = 0$, (b) 1000, and (c) 40,000 with the initial condition $\phi(x, y, z, 0) = 0.05 + (0.285 - 0.05)\left(\frac{x+100}{200}\right)^3 + \text{rand}(x, y, z)$.

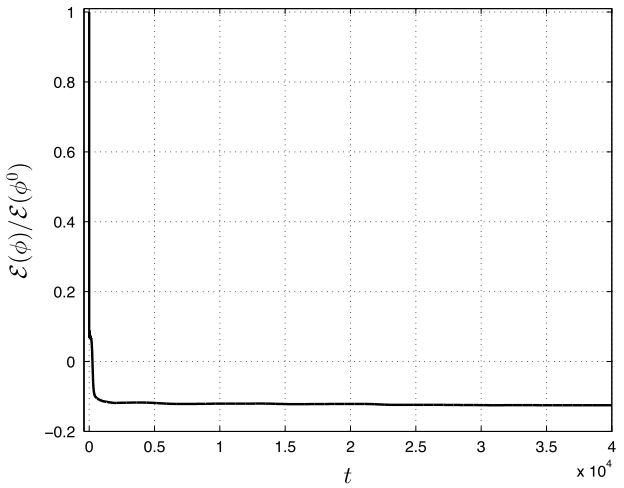

Fig. 16. Evolution of $\mathcal{E}(\phi)/\mathcal{E}(\phi^0)$.

The computational domain is $\Omega = [-100, 100] \times [-20, 20] \times [-20, 20]$. Fig. 15 shows the evolution of $\phi(x, y, z, t)$. In this simulation, we obtain a mixed pattern of striped and hexagonal. Fig. 16 shows the evolution of the energy. We observe that the energy is non-increasing.

4.7. Effect of surface topology on pattern formation

In order to investigate the effect of surface topology on pattern formation, we consider two rectangular parallelepipeds having the following signed distance functions: $\psi_{64,8,8}(x, y, z)$ and $\psi_{64,4,4}(x, y, z)$ on a domain $\Omega = [-36, 36]^3$, where

$$\psi_{u,v,w}(x, y, z) = \min(\max(|x| - u/2, \max(|y| - v/2, |z| - w/2)), 0) + \sqrt{\max(|x| - u/2, 0)^2 + \max(|y| - v/2, 0)^2 + \max(|z| - w/2, 0)^2}.$$

Note that Fig. 11 shows a hexagonal pattern on the cube having $\psi_{64,64,64}(x, y, z)$ with $\bar{\phi} = 0.15$. Figs. 17 and 18 show the evolution of $\phi(x, y, z, t)$ on the rectangular parallelepipeds having $\psi_{64,8,8}(x, y, z)$ and $\psi_{64,4,4}(x, y, z)$ with $\bar{\phi} = 0.15$, respectively. On the rectangular parallelepiped having $\psi_{64,8,8}(x, y, z)$, we also obtain a hexagonal pattern. However, on the rectangular parallelepiped having $\psi_{64,4,4}(x, y, z)$ (a narrow rectangular parallelepiped), we obtain a striped pattern even with $\bar{\phi} = 0.15$. Fig. 19 shows the evolution of the energy on the rectangular parallelepipeds having $\psi_{64,8,8}(x, y, z)$ and $\psi_{64,4,4}(x, y, z)$ with $\bar{\phi} = 0.15$. We observe that the energy is non-increasing.

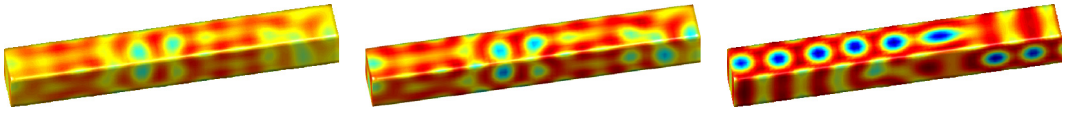

(a) $t = 250$. (b) $t = 350$. (c) $t = 10{,}000$.

Fig. 17. Evolution of $\phi(x, y, z, t)$ on the rectangular parallelepiped having $\psi_{64,8,8}(x, y, z)$ with $\bar{\phi} = 0.15$.

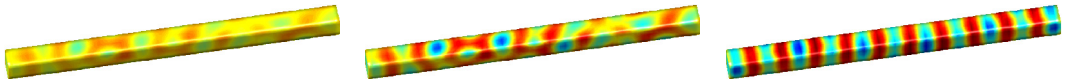

(a) $t = 250$. (b) $t = 350$. (c) $t = 10{,}000$.

Fig. 18. Evolution of $\phi(x, y, z, t)$ on the rectangular parallelepiped having $\psi_{64,4,4}(x, y, z)$ with $\bar{\phi} = 0.15$.

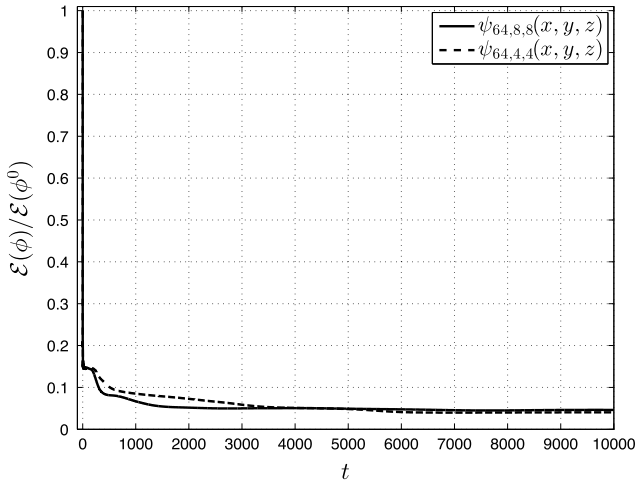

Fig. 19. Evolution of $\mathcal{E}(\phi)/\mathcal{E}(\phi^0)$ on the rectangular parallelepipeds having $\psi_{64,8,8}(x, y, z)$ and $\psi_{64,4,4}(x, y, z)$ with $\bar{\phi} = 0.15$.

5. Conclusions

We presented a simple and efficient finite difference method for the PFC equation on curved surfaces embedded in $\mathbb{R}^3$. We employed a three-dimensional narrow band neighborhood of a curved surface that is defined as a zero level set of a signed distance function. The PFC equation on the surface was extended to the three-dimensional narrow band domain. By using the closest point method and applying a pseudo-Neumann boundary condition, we could use the standard seven-point discrete Laplacian operator instead of the discrete Laplace–Beltrami operator on the surface. The PFC equation on the narrow band domain was discretized using an unconditionally stable scheme and the resulting implicit discrete system of equations was solved by using the Jacobi iterative method. We performed numerical experiments on various curved surfaces, which demonstrate the efficiency and usefulness of the proposed method for the PFC equation on curved surfaces.

Acknowledgments

The authors thank the reviewers for the constructive and helpful comments on the revision of this article. The first author (H.G. Lee) was supported by Basic Science Research Program through the National Research Foundation of Korea (NRF) funded by the Ministry of Education (2009-0093827). The corresponding author (J.S. Kim) was supported by the National Research Foundation of Korea (NRF) grant funded by the Korea government (MSIP) (NRF-2014R1A2A2A01003683).

References

[1] K.R. Elder, M. Grant, Modeling elastic and plastic deformations in nonequilibrium processing using phase field crystals, Phys. Rev. E 70 (2004) 051605.
[2] K.R. Elder, M. Katakowski, M. Haataja, M. Grant, Modeling elasticity in crystal growth, Phys. Rev. Lett. 88 (2002) 245701.
[3] N. Provatas, J.A. Dantzig, B. Athreya, P. Chan, P. Stefanovic, N. Goldenfeld, K.R. Elder, Using the phase-field crystal method in the multi-scale modeling of microstructure evolution, JOM 59 (2007) 83–90.
[4] J. Swift, P.C. Hohenberg, Hydrodynamic fluctuations at the convective instability, Phys. Rev. A 15 (1977) 319.
[5] R. Backofen, A. Rätz, A. Voigt, Nucleation and growth by a phase field crystal (PFC) model, Phil. Mag. Lett. 87 (2007) 813–820.
[6] M. Cheng, J.A. Warren, An efficient algorithm for solving the phase field crystal model, J. Comput. Phys. 227 (2008) 6241–6248.
[7] M. Dehghan, V. Mohammadi, The numerical simulation of the phase field crystal (PFC) and modified phase field crystal (MPFC) models via global and local meshless methods, Comput. Methods Appl. Mech. Engrg. 298 (2016) 453–484.
[8] H. Gomez, X. Nogueira, An unconditionally energy-stable method for the phase field crystal equation, Comput. Methods Appl. Mech. Engrg. 249–252 (2012) 52–61.
[9] Z. Hu, S.M. Wise, C. Wang, J.S. Lowengrub, Stable and efficient finite-difference nonlinear-multigrid schemes for the phase field crystal equation, J. Comput. Phys. 228 (2009) 5323–5339.
[10] H.G. Lee, J. Shin, J.-Y. Lee, First and second order operator splitting methods for the phase field crystal equation, J. Comput. Phys. 299 (2015) 82–91.
[11] P. Vignal, L. Dalcin, D.L. Brown, N. Collier, V.M. Calo, An energy-stable convex splitting for the phase-field crystal equation, Comput. Struct. 158 (2015) 355–368.
[12] S.M. Wise, C. Wang, J.S. Lowengrub, An energy-stable and convergent finite-difference scheme for the phase field crystal equation, SIAM J. Numer. Anal. 47 (2009) 2269–2288.
[13] Z. Zhang, Y. Ma, Z. Qiao, An adaptive time-stepping strategy for solving the phase field crystal model, J. Comput. Phys. 249 (2013) 204–215.
[14] S. Aland, J. Lowengrub, A. Voigt, A continuum model of colloid-stabilized interfaces, Phys. Fluids 23 (2011) 062103.
[15] S. Aland, A. Rätz, M. Röger, A. Voigt, Buckling instability of viral capsids–a continuum approach, Multiscale Model. Simul. 10 (2012) 82–110.
[16] A. Rätz, A. Voigt, PDE's on surfaces–a diffuse interface approach, Commun. Math. Sci. 4 (2006) 575–590.
[17] P. Tang, F. Qiu, H. Zhang, Y. Yang, Phase separation patterns for diblock copolymers on spherical surfaces: A finite volume method, Phys. Rev. E 72 (2015) 016710.
[18] Y. Choi, D. Jeong, S. Lee, M. Yoo, J. Kim, Motion by mean curvature of curves on surfaces using the Allen–Cahn equation, Internat. J. Engrg. Sci. 97 (2015) 126–132.
[19] D. Jeong, J. Kim, Microphase separation patterns in diblock copolymers on curved surfaces using a nonlocal Cahn–Hilliard equation, Eur. Phys. J. E 38 (2015) 117.
[20] S.J. Ruuth, B. Merriman, A simple embedding method for solving partial differential equations on surfaces, J. Comput. Phys. 227 (2008) 1943–1961.
[21] M. Bertalmío, L.-T. Cheng, S. Osher, G. Sapiro, Variational problems and partial differential equations on implicit surfaces, J. Comput. Phys. 174 (2001) 759–780.
[22] J.B. Greer, An improvement of a recent Eulerian method for solving PDEs on general geometries, J. Sci. Comput. 29 (2006) 321–352.